Inorganic Chemistry

ARTICLE

pubs.acs.org/IC

Stepwise 1D Growth of Luminescent Au(I)−Ag(I) Phosphine−Alkynyl Clusters: Synthesis, Photophysical, and Theoretical Studies

Igor O. Koshevoy,*[,†] Chia-Li Lin,[‡] Antti J. Karttunen,[†] Janne Jänis,[†] Matti Haukka,[†] Sergey P. Tunik,[§] Pi-Tai Chou,*[,‡] and Tapani A. Pakkanen*[,†]

[†]Department of Chemistry, University of Eastern Finland, Joensuu, 80101, Finland

[‡]National Taiwan University, Department of Chemistry, Taipei 106, Taiwan

[§] Department of Chemistry, St.-Petersburg State University, Universitetskii pr. 26, 198504, St. Petersburg, Russia

Supporting Information

ABSTRACT: Reactions between the diphosphino-gold cationic complexes $[Au_2(PPh_2\text{-}C_2\text{-}(C_6H_4)_n\text{-}C_2\text{-}PPh_2)_2]^{2+}$ (n = 0, 1, 2, 3) and polymeric acetylides $(AuC_2Ph)_n$ and $(AgC_2Ph)_n$ lead to the formation of a new family of heterometallic clusters with the general formula $[Au_{8+2n}Ag_{6+2n}(C_2Ph)_{8+4n}(PPh_2C_2(C_6H_4)_nC_2PPh_2)_2]^{2+}$, n = 0 (**1**), 1 (**2**), 2 (**3**), 3 (**4**). Compounds **1**−**4** were characterized in detail by NMR and ESI-MS spectroscopy. Complex **1** (n = 0) crystallizes in two forms (orange (**1a**) and yellow (**1b**)), one of which (**1a**) has been analyzed by X-ray crystallography. The luminescence behavior of **1**−**4** has been studied. Compounds **2** and **3** exhibited orange-red phosphorescence with quantitive quantum efficiency in both aerated and degassed CH_2Cl_2, implying O_2-independent phosphorescence due to efficient protection of the emitting chromophore center by the organic ligands. Complex **3** exhibits reasonable two-photon absorption (TPA) property with a cross section of $\sigma \approx 45$ GM (800 nm), which is comparable to the value of commercially available TPA dyes such as coumarin 151. Computational studies have been performed to correlate the structural and photophysical features of the complexes studied. The metal-centered triplet emission within the heterometallic core is suggested to play a key role in the observed phosphorescence. The luminescence spectrum of **1** in CH_2Cl_2 shows dual phosphorescence maximized at 575 nm (the P_1 band) and 770 nm (the P_2 band). Both P_1 and P_2 bands possess identical excitation spectra, i.e., the same ground-state origin, and the same relaxation dynamics throughout the temperature range of 298−200 K. The dual emission of **1** arises from fast structural fluctuation upon excitation, perhaps forming two geometry isomers, which exhibit distinctly different P_1 and P_2 bands. The scrambling dynamics might require large-amplitude motion and, hence, is hampered in rigid media, as evidenced by the single emission for **1a** (610 nm) and **1b** (570 nm) observed in solid.

INTRODUCTION

The heteronuclear complexes of group 11 metals attract considerable attention, because of the rich variety of structural patterns they adopt, theoretical interest to the metal−metal interactions, and promising photophysical characteristics, which have the potential for modern technological applications (e.g., OLED displays, luminescent sensors, and bioimaging labels). These species often show a trend to form multiple heterometallophilic bonds responsible for the unexpected structural architectures and, consequently, rise or change of the photoemissive properties, which are strongly dependent on the distances between the interacting metals, the nature and number of the constituting ligands, and the coordination geometry of the metal centers.[1] In our recent studies, we were mainly focused on the heterometallic Au^I, Ag^I, Cu^I alkynyl−phosphine complexes, which demonstrate very strong room-temperature phosphorescence with a small to negligible oxygen quenching effect.[2−4] The dominating structural motif—an $[Au_xM_y(C_2R)_{2x}]$ cluster inside the triangular $[Au_3(PP)_3]^{3+}$ "belt" (where *PP* = linear rigid diphosphine)—was found for both Au^I−Cu^I and Au^I−Ag^I bimetallic species.[5−7] However, it has been already mentioned that numerous Au^I−Ag^I compounds were synthesized without analogy with the Au^I−Cu^I ones.[8] This increasing structural diversity of the gold−silver complexes was also confirmed by some of our reports.[3,4] Thus, variation of the synthetic strategy allowed for the selective preparation of two structurally different Au^I−Ag^I clusters (see Scheme 1), which also demonstrated sharp contrast of their emissive properties.[3,6]

Inspired by the attractive luminescent characteristics of **I**, we intended to expand the family of the related compounds; however, we unexpectedly were unable to obtain its congeners by modifying the oligophenylene-based diphosphines or varying the substituents of the phenylalkynyl ligands. Alternatively, our interest switched to the family of dialkynyl-based P-ligands, $PPh_2\text{-}C_2\text{-}(C_6H_4)_n\text{-}C_2\text{-}PPh_2$ (n = 0−3), which, in comparison to $PPh_2\text{-}(C_6H_4)_n\text{-}PPh_2$ diphosphines, have (a) slightly different spatial separation of the P atoms and (b) significantly different electron-donating properties. These electronic and stereochemical variations of the ligands, together with theoretical calculations on the stability of the expected heterometallic products, suggest that the $PPh_2\text{-}C_2\text{-}(C_6H_4)_n\text{-}C_2\text{-}PPh_2$ phosphines could be the promising candidates in the synthesis of the clusters topologically similar to **I**.

Herein, we report on the reactions between the diphosphino-gold cationic complexes $[Au_2(PPh_2(C_6H_4)_nPPh_2)_2]^{2+}$ (n = 0, 1,

Received: November 2, 2010
Published: February 08, 2011

Scheme 1. Formation of Two Types of Au^I-Ag^I Aggregates

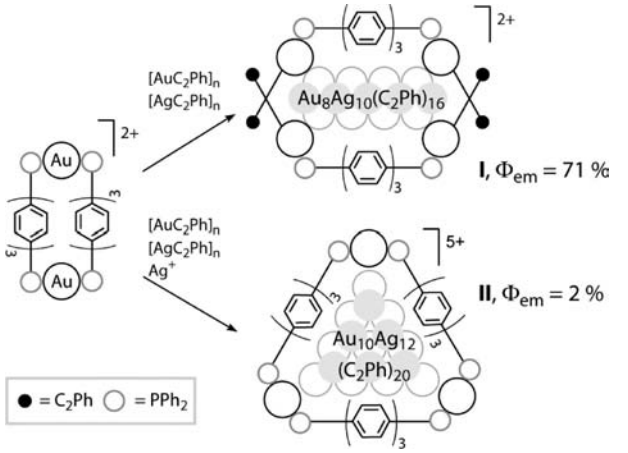

2, 3) and polymeric acetylides $(AuC_2Ph)_n$ and $(AgC_2Ph)_n$, leading to the formation of a new family of large heterometallic clusters with the general formula $[Au_{8+2n}Ag_{6+2n}(C_2Ph)_{8+4n}(PPh_2C_2(C_6H_4)_nC_2PPh_2)_2]^{2+}$, n = 0 (**1**), 1 (**2**), 2 (**3**), 3 (**4**). Details of the synthesis route, characterization, and associated photophysical properties are elaborated as follows.

EXPERIMENTAL SECTION

General Comments. $(AuC_2Ph)_n$,[9] $(AgC_2Ph)_n$,[10] $PPh_2C_2C_2PPh_2$ (***P*^{0}*P***),[11] 1,4-$PPh_2C_2C_6H_4C_2PPh_2$ (***P*^{1}*P***),[7] 4,4′-$PPh_2C_2(C_6H_4)_2C_2$-PPh_2 (***P*^{2}*P***),[7] and 4,4″-diiodoterphenyl[12] were synthesized according to published procedures. Complexes $[Au_2(PP)_2]^{2+}$ (where *PP* = diphosphine) were prepared in a manner similar to the published analogues.[2,3] $[Au_2(P^0P)_2](PF_6)_2$ has limited stability in solution; therefore, its preparation should be carried out as fast as possible. Tetrahydrofuran was distilled over Na-benzophenoneketyl under nitrogen atmosphere prior to use. Other reagents and solvents were used as received. The solution 1D ^1H, ^{31}P NMR and $^1H-^1H$ COSY spectra were recorded on Bruker Avance 400 spectrometer. Mass spectra were measured on a Bruker APEX-Qe ESI FT-ICR instrument, in the positive-ion mode. Microanalyses were carried out in the analytical laboratory of the University of Eastern Finland.

4,4″-HC_2-$(C_6H_4)_3$-C_2H. 4,4″-Diiodoterphenyl (4.6 g, 9.54 mmol) was suspended in THF (40 cm^3), diluted with degassed NEt_3 (30 cm^3) under a nitrogen atmosphere, and $Pd(PPh_3)_2Cl_2$ (150 mg, 0.214 mmol), CuI (50 mg, 0.262 mmol) and (trimethylsilyl)acetylene (2.5 g, 25.5 mmol) were added. The reaction mixture was stirred overnight at room temperature, evaporated, washed with methanol (2 × 20 cm^3) and dried. Brownish solid was dissolved in $CHCl_3$ (ca. 120 cm^3), passed through a silica gel (2.5 × 10 cm), evaporated and washed with diethyl ether/methanol 1:1 v/v mixture (2 × 10 cm^3) to give creamy crystalline solid of 4,4″-bis(trimethylsilylethynyl)terphenyl (3.85 g, 96%). Deprotection was carried out by suspending the intermediate in THF/methanol 5:3 v/v mixture (80 cm^3) and stirring with K_2CO_3 (2 g) under a nitrogen atmosphere for 12 h. The reaction mixture was evaporated and washed with H_2O (20 cm^3). Solid residue was extracted with hot $CHCl_3$ (4 × 70 cm^3), passed through a layer of silica gel (150 mesh, 2.5 × 10 cm), evaporated and briefly washed with ethanol (15 cm^3) to give pale-creamy crystalline product (2.46 g, total yield 93%). ^1H NMR ($CDCl_3$; δ): 7.68 (s, 4H, $-C_6H_4-$), 7.60 (m, 8H, $-C_6H_4-C_2H$), 3.15 (s, 2H, $-C_2H$). Anal. Calc. for $C_{22}H_{14}$: C, 94.93; H, 5.07. Found: C, 94.62; H, 5.27.

4,4″-PPh_2C_2-$(C_6H_4)_3$-C_2PPh_2 (*P*^{3}*P*). The synthesis was carried out under a nitrogen atmosphere. A solution of 4,4″-diethynylterphenyl (0.5 g, 1.80 mmol) in THF (60 cm^3) was cooled to −78 °C and a 1.6 M solution of *n*-BuLi in hexanes (2.6 cm^3, 4.16 mmol) was added dropwise within 5 min under stirring. The resulting pale greenish suspension was warmed up to −10 °C within ca. 3 h, stirred for 0.5 h, then cooled to −78 °C again and treated dropwise with PPh_2Cl (0.9 g, 4.08 mmol). The reaction mixture changed to a yellow solution and was stirred below −60 °C for 1 h, then allowed slowly (ca. 2 h) to reach room temperature, and stirred overnight. The solvents were evaporated, and the brownish solid residue was washed with methanol (3 × 15 cm^3) and vacuum-dried. Crude ***P*^{3}*P*** was dissolved in hot $CHCl_3$ (ca. 30 cm^3), treated with activated charcoal, diluted with hexanes (7 cm^3), passed through a silica gel (150 mesh, 2.5 × 15 cm, eluent $CHCl_3$/hexanes 4:1 v/v). Pale yellow solution was evaporated, the solid obtained was washed with THF−methanol mixture 1:2 v/v (2 × 9 cm^3), diethyl ether (2 × 5 cm^3) to give pale yellowish ligand (0.71 g, 61%). Mp. 211−212 °C. $^{31}P\{^1H\}$ NMR ($CDCl_3$; δ): −33.8 (s). ^1H NMR ($CDCl_3$; δ): 7.72−7.67 (m, 12H), 7.64(s, 8H), 7.41−7.35 (m, 12H). Anal. Calc. for $C_{46}H_{32}P_2$: C, 85.43; H, 4.99. Found: C, 84.94; H, 4.96.

$[Au_8Ag_6(C_2Ph)_{12}(PPh_2$-$C_2$-$C_2$-$PPh_2)_2](PF_6)_2$ (1). $(AuC_2Ph)_n$ (69 mg, 0.232 mmol) and $(AgC_2Ph)_n$ (48 mg, 0.230 mmol) were suspended in CH_2Cl_2 (20 cm^3), stirred for 10 min and $[Au_2(P^0P)_2](PF_6)_2$ (50 mg, 0.033 mmol) was added. The reaction mixture was stirred overnight in the absence of light, resulting in a dirty yellow solution and some insoluble residue. The solution was filtered and evaporated, and crude **1** was repetitiously recrystallized via the gas-phase diffusion of diethyl ether into its solution in CH_2Cl_2/acetone/MeOH at +5 °C to give bright orange crystals (136 mg, 91%). Crystallization of **1** via gas-phase diffusion of diethyl ether into its acetone solution at +5 °C results in the formation of a yellow microcrystalline form. Upon dissolution, the orange and yellow forms show identical spectral characteristics. ES MS (*m*/*z*): $[Au_8Ag_6(C_2Ph)_{12}(PPh_2C_2C_2PPh_2)_2]^{2+}$ 2136.4 (calcd 2136.4). $^{31}P-\{^1H\}$ NMR (CD_2Cl_2; δ): 16.2 (s, 4P), −143.0 (sept, $2PF_6$). ^1H NMR (CD_2Cl_2; δ): **diphosphine**: ***PPh*-1**, 7.85, ortho-H, 8H, (dd, J(HH) 7.1 J(PH) 14.7 Hz), 7.64, para-H, 4H, (t, J(HH) 7.6 Hz), 7.55 meta-H, 8H, (ddd, J(HH) 7.1, 7.6 J(PH) 3.0 Hz); ***PPh*-2**, 7.75, ortho-H, 8H, (dd, J(HH) 7.1 J(PH) 14.9 Hz), 7.31, para-H, 4H, (t, J(HH) 7.6 Hz), 7.15 meta-H, 8H, (dd, J(HH) 7.1, 7.6); **$[Au(C_2Ph)_2]$ rods:** (**terminal**) 7.67 ortho-H, 8H (d, J(HH) 7.1 Hz), 7.35, para-H, 4H, (t, J(HH) 7.5 Hz), 7.20, meta-H, 8H, (dd, J(HH) 7.5, 7.1 Hz), (**A**) 7.14, para-H, 4H, (t, J(HH) 7.8 Hz), 6.72, meta-H, 8H, (dd, J(HH) 7.8, 7.2 Hz), 6.23 ortho-H, 8H (d, J(HH) 7.2 Hz), (**B**) 7.11, para-H, 4H, (t, J(HH) 7.8 Hz), 6.72, meta-H, 8H, (dd, J(HH) 7.1, 7.8 Hz), 7.04 ortho-H, 8H (d, J(HH) 7.1 Hz). Anal. Calc. for $Ag_6Au_8C_{152}H_{100}F_{12}P_6$: C, 40.01; H, 2.21. Found: C, 39.49; H 2.40.

$[Au_{10}Ag_8(C_2Ph)_{16}(PPh_2$-$C_2-C_6H_4-C_2$-$PPh_2)_2](CF_3SO_3)_2$ (2). $(AuC_2Ph)_n$ (101 mg, 0.339 mmol) and $(AgC_2Ph)_n$ (71 mg, 0.340 mmol) were suspended in CH_2Cl_2 (20 cm^3), stirred for 10 min, and then $[Au_2(P^1P)_2](CF_3SO_3)_2$ (86 mg, 0.051 mmol) was added. The reaction mixture was stirred for 1 h in the absence of light, resulting in a bright yellow−orange solution and small amount of yellow residue. The solution was filtered and evaporated, and crude **2** was washed with acetone−hexane (3:2 v/v) mixture (3 × 5 cm^3). Recrystallization by gas-phase diffusion of diethyl ether into its CH_2Cl_2/THF solution at −7 °C gave mainly an orange crystalline material, together with yellow-greenish crystals identified as $[Au_9Ag_6(C_2Ph)_{12}(PPh_2C_2C_6H_4C_2PPh_2)_3](CF_3SO_3)_3$.[7] The latter was removed by washing the solid with acetone/hexane 3:2 v/v mixture (4 × 5 cm^3) and THF (3 × 5 cm^3). Orange powder (138 mg, 57%). Pure **2** is unstable in solution at room temperature. ES MS (*m*/*z*): $[Au_{10}Ag_8(C_2Ph)_{16}(PPh_2C_2C_6H_4C_2PPh_2)_2]^{2+}$ 2719.9 (calcd 2719.9). $^{31}P\{^1H\}$ NMR (CD_2Cl_2; δ): 13.3 (s). ^1H NMR (CD_2Cl_2; δ): **diphosphine**:

7.90,−≡−C_6H_4−≡−, 8H (s), ***PPh-1***, 7.80, ortho-H, 8H, (dd, J(HH) 7.0 J(PH) 14.5 Hz), 7.51, para-H, 4H, (t, J(HH) 7.4 Hz), 7.44 meta-H, 8H, (ddd, J(HH) 7.0, 7.4 J(PH) 2.8 Hz); ***PPh-2***, 7.70, ortho-H, 8H, (dd, J(HH) 7.0 J(PH) 14.6 Hz), 7.14 meta-H, 8H, (dd, J(HH) 7.0, 7.5), 7.12, para-H, 4H, (t, J(HH) ca. 7.5 Hz); [**Au(C_2Ph)$_2$**] **rods:** (**terminal**) 7.57 ortho-H, 8H (d, J(HH) ca. 7.5 Hz), 7.24, meta-H, 8H, (dd, J(HH) ca. 7.5, 8.0 Hz), 7.08, para-H, 4H, (t, J(HH) ca. 8 Hz); (**A**) 6.62, meta-H, 8H, (dd, J(HH) 7.0, 8.0 Hz), 7.06 ortho-H, 8H (d, J(HH) 7.0 Hz), 7.12, para-H, 4H, (t, J(HH) 8.0 Hz); (**B**) 6.44, meta-H, 8H, (dd, J(HH) 7.0, 7.6 Hz), 6.79 ortho-H, 8H (d, J(HH) 7.0 Hz), 6.89, para-H, 4H, (t, J(HH) 7.6 Hz); (**C**) 6.96, para-H, 4H, (t, J(HH) 7.6 Hz), 6.57, meta-H, 8H, (dd, J(HH) 7.1, 7.6 Hz), 5.97 ortho-H, 8H (d, J(HH) 7.1 Hz). Anal. Calc. for $Ag_8Au_{10}C_{198}H_{128}F_6O_6P_4S_2$: C, 41.45; H, 2.25. Found: C, 41.56; H 2.52.

[$Au_{12}Ag_{10}(C_2Ph)_{20}(PPh_2$-$C_2$-$(C_6H_4)_2$-$C_2$-$PPh_2)_2](CF_3SO_3)_2$ (3). $(AuC_2Ph)_n$ (100 mg, 0.336 mmol) and $(AgC_2Ph)_n$ (70.5 mg, 0.337 mmol) were suspended in CH_2Cl_2 (20 cm^3), stirred for 10 min, and then $[Au_2(P^2P)_2](CF_3SO_3)_2$ (68 mg, 0.037 mmol) was added. The reaction mixture was stirred for 1.5 h in the absence of light, resulting in an almost-transparent bright yellow solution. The solution was filtered and evaporated, and crude **3** was recrystallized via slow evaporation of its CH_2Cl_2/acetone/heptane solution at +5 °C to give a yellow crystalline material, which was dissolved in CH_2Cl_2 (4 cm^3), diluted with acetone/hexane 1:1 v/v mixture (4 cm^3), filtered, and precipitated via the addition of an excess of hexanes. The bright yellow powder was washed with an acetone/hexane 3:1 v/v mixture (2 × 5 cm^3) and diethyl ether (2 × 5 cm^3) and then dried (210 mg, 91%). ES MS (m/z): $[Au_{12}Ag_{10}(C_2Ph)_{20}(PPh_2C_2(C_6H_4)_2C_2PPh_2)_2]^{2+}$ 3303.0 (calcd 3302.9). $^{31}P\{^1H\}$ NMR (CD_2Cl_2; δ): 12.6 (s). ^1H NMR (CD_2Cl_2; δ): **diphosphine**: 7.96, −≡−(C_6H_4)$_2$−≡−, 16H (AB system), ***PPh-1***, 7.81 ortho-H, 8H, (dd, J(HH) 7.1 J(PH) 14.4 Hz), 7.49 para-H, 4H, (t, J(HH) ca. 7.5 Hz), 7.43 meta-H, 8H, (ddd, J(HH) 7.1, ca. 7.5 J(PH) 2.3 Hz); ***PPh-2***, 7.75 ortho-H, 8H, (dd, J(HH) 7.2 J(PH) 14.6 Hz), 7.28 para-H, 4H, (t, J(HH) ca. 7.5 Hz), 7.14 meta-H, 8H, (dd, J(HH) 7.2, 7.5); [**Au(C_2Ph)$_2$**] **rods:** (**terminal**) 7.50 ortho-H, 8H (d, J(HH) 7.1 Hz), 7.19, para-H, 4H, (t, J(HH) 7.5 Hz); 7.03, meta-H, 8H, (dd, J(HH) 7.5, 7.1 Hz), (**A**) 7.00, para-H, 4H, (t, J(HH) ca. 7.5 Hz), 7.00 ortho-H, 8H (d, J(HH) 7.4 Hz), 6.61, meta-H, 8H, (dd, J(HH) 7.5 7.4 Hz); (**B**) 6.94, para-H, 4H, (t, J(HH) 7.5 Hz), 6.57, meta-H, 8H, (dd, J(HH) 7.5, 7.5 Hz), 5.92 ortho-H, 8H (d, J(HH) 7.5 Hz); (**C**) 6.83, para-H, 4H, (t, J(HH) 7.5 Hz), 6.67 ortho-H, 8H (d, J(HH) 7.3 Hz), 6.41, meta-H, 8H, (dd, J(HH) 7.5, 7.3 Hz); (**D**) 6.82−6.77, m, para-H and ortho-H, 12H, 6.39, meta-H, 8H, (dd, J(HH) ca. 7.8 Hz). Anal. Calc. for $Ag_{10}Au_{12}C_{242}H_{156}F_6O_6P_4S_2$: C, 42.10; H, 2.28. Found: C, 42.00; H 2.53.

[$Au_{14}Ag_{12}(C_2Ph)_{24}(PPh_2$-$C_2$-$(C_6H_4)_3$-$C_2$-$PPh_2)_2](CF_3SO_3)_2$ (4). $(AuC_2Ph)_n$ (150 mg, 0.503 mmol) and $(AgC_2Ph)_n$ (105 mg, 0.502 mmol) were suspended in CH_2Cl_2 (25 cm^3), stirred for 10 min and then $[Au_2(P^3P)_2](CF_3SO_3)_2$ (108 mg, 0.054 mmol) was added. The reaction mixture was stirred for 1.5 h in the absence of light, resulting in a bright yellow solution and some yellow insoluble residue. The workup procedure, which was identical to that of **3**, gave **4** as a yellow powder (195 mg, 56%). Pure **4** is very unstable in solution at room temperature. ES MS (m/z): $[Au_{14}Ag_{12}(C_2Ph)_{24}(PPh_2C_2(C_6H_4)_3C_2PPh_2)_2]^{2+}$ 3885.9 (calcd 3885.9). $^{31}P\{^1H\}$ NMR (CD_2Cl_2; δ): 12.4 (s). ^1H NMR (CD_2Cl_2; δ): **diphosphine**: 8.08, −≡−(C_6H_4) −(C_6H_4)−(C_6H_4)−≡−, s, 8H; 8.01,−≡−(C_6H_4)−(C_6H_4) −(C_6H_4)−≡−, 16H (AB system), ***PPh-1***, 7.83 ortho-H, 8H, (dd, J(HH) 7.6 J(PH) 15.0 Hz), 7.52−7.39 m, meta + para-H, 12H; ***PPh-2***, 7.81 ortho-H, 8H, (dd, J(HH) 7.6 J(PH) 15.0 Hz), 7.26 para-H, 4H, (t, J(HH) ca. 7.5 Hz), 7.15 meta-H, 8H, (dd, J(HH) 7.6, 7.5); [**Au(C_2Ph)$_2$**] **rods:** (**terminal**) 7.47 ortho-H, 8H (d, J(HH) 7.1 Hz), 7.19, para-H, 4H, (t, J(HH) 7.5 Hz); 7.06, meta-H, 8H, (dd, J(HH) 7.5, 7.1 Hz), (**A**) 7.08 ortho-H, 8H (d, J(HH) ca. 7.5 Hz), 6.94, para-H, 4H, (t, J(HH) 7.6 Hz), 6.52, meta-H, 8H, (dd, J(HH) 7.5 7.6 Hz); (**B**) 6.90, para-H, 4H, (t, J(HH) 7.3 Hz), 6.53, meta-H, 8H, (dd, J(HH) 7.3, 7.4 Hz), 5.77 ortho-H, 8H (d, J(HH) 7.4 Hz); (**C**) 6.66, para-H, 4H, (t, J(HH) 7.6 Hz), 6.55 ortho-H, 8H (d, J(HH) ca. 7.6 Hz), 6.29, meta-H, 8H, (dd, J(HH) 7.6 Hz); (**D**) 6.78, para-H, 4H, (t, J(HH) 7.6 Hz), 6.56 ortho-H, 8H (d, J(HH) ca. 7.6 Hz), 6.43, meta-H, 8H, (dd, J(HH) 7.6 Hz); (**E**) 6.74, para-H, 4H, (t, J(HH) 7.6 Hz), 6.69 ortho-H, 8H (d, J(HH) ca. 7.6 Hz), 6.39, meta-H, 8H, (dd, J(HH) 7.6 Hz). Anal. Calc. for $Ag_{12}Au_{14}C_{286}H_{184}F_6O_6P_4S_2$: C, 42.56; H, 2.30. Found: C, 42.43; H, 2.20.

Photophysical Measurements. Steady-state absorption and emission measurements, both in solution and in the solid state, were recorded on a Hitachi (U-3310) spectrophotometer and an Edinburgh (FS920) fluorometer, respectively. Both the wavelength-dependent excitation and emission response of the fluorometer have been calibrated. To determine the photoluminescence quantum yield in solution, the samples were degassed by three freeze−pump−thaw cycles. 4--(Dicyanomethylene)-2-methyl-6-(paradimethylaminostyryl)-4H-pyran (DCM, λ_{max} = 615 nm, Exciton) in methanol, with a quantum yield of ~0.4, served as the standard for measuring the quantum yield. Solid-state quantum yields were determined with a calibrated integrating sphere system. The uncertainty of the quantum yield measurement was in the range of <2% (an average of three replica). Lifetime studies were performed with an Edinburgh FL 900 photon-counting system, using a hydrogen-filled lamp as the excitation source. The emission decays were fitted by the sum of exponential functions with a temporal resolution of ~300 ps by the deconvolution of instrument response function.

The two-photon absorption cross section was measured using an open-aperture Z-scan experiment.[13] Briefly, in this study, a mode-locked Ti:sapphire laser (Tsunami, Spectra Physics) was coupled to a regenerative amplifier that generated ~180 fs, 1 mJ pulses (800 nm, 1 kHz, Spitfire Pro, Spectra Physics). The pulse energy, after proper attenuation, was reduced to 0.75−1.5 μJ and the repetition rate was further reduced to 20 Hz to eliminate excited-state absorption. The laser beam was focused through a 2.00 mm cell filled with the sample solution (1.3 × 10^{-3} M). When the sample cell was translated along the beam direction (z-axis), the transmitted laser intensity was detected. The TPA-induced decrease in transmittance, $T(z)$, can be fitted with eqs 1 and 2, in which the TPA coefficient (β) is incorporated:[14]

$$T(z) = \sum_{n=0}^{\infty} \frac{(-q)^n}{(n+1)^{3/2}} \quad (1)$$

$$q = \frac{\beta I_0 L}{1 + (z^2/z_0^2)} \quad (2)$$

where n is an integer number from 0 to ∞ and has been truncated at n = 1000, L is the sample length, I_0 is the input intensity, z represents the sample position with respect to the focal point, and z_0 denotes the diffraction length of the incident beam (Rayleigh range). After obtaining β, the TPA cross section (σ_2) can be deduced using the equation

$$\beta = \frac{\sigma_2 N_A d \times 10^{-3}}{h\nu} \quad (3)$$

where N_A is the Avogadro constant, d the sample concentration, and $h\nu$ the incident photon energy.

X-ray Structure Determinations. The crystal of **1** was immersed in cryo-oil, mounted in a Nylon loop, and measured at a temperature of 100 K. The X-ray diffraction (XRD) data was collected on a Bruker AXS Smart ApexII diffractometer, using Mo Kα radiation (λ = 0.71073 Å). The APEX2[15] program package was used for cell refinements and data reductions. The structure was solved by direct methods using the SHELXS-97[16] program with the WinGX[17] graphical user interface. A numerical absorption correction (SADABS)[18] was applied to the data. Structural refinement was carried out using

Table 1. Crystal Data of 1

	1
empirical formula	$C_{154}H_{110}Ag_6Au_8F_{12}O_3P_6$
fw	4645.19
temp (K)	100(2)
λ (Å)	0.71073
cryst syst	orthorhombic
space group	*Pbcn*
a (Å)	18.0224(4)
b (Å)	28.5223(6)
c (Å)	28.2868(7)
V (Å^3)	14540.6(6)
Z	4
ρ_{calc} (Mg/m^3)	2.122
μ(Mo Kα) (mm^{-1})	8.956
No. reflns.	127402
Unique reflns.	19909
GOOF (F^2)	1.030
R_{int}	0.0783
$R1^a$ ($I \geq 2\sigma$)	0.0360
$wR2^b$ ($I \geq 2\sigma$)	0.0777

$^a R1 = \sum||F_o| - |F_c||/\sum|F_o|$. $^b wR2 = [\sum[w(F_o^2 - F_c^2)^2]/\sum[w(F_o^2)^2]]^{1/2}$.

SHELXL-97.[16] The asymmetric unit of **1** contains a half a molecule. The water of crystallization was partially lost; therefore, it was refined with an occupancy of 0.5. The H_2O and OH hydrogen atoms were located from the difference Fourier map but constrained to ride on their parent atom, with $U_{iso} = 1.5U_{eq}$ (parent atom). Other hydrogen atoms were positioned geometrically and were also constrained to ride on their parent atoms, with C−H = 0.95−0.98 Å, and $U_{iso} = 1.2-1.5\ U_{eq}$ (parent atom). The crystallographic details are summarized in Table 1.

Computational Details. The geometries of complexes **1**−**4** were optimized using the BP86 density functional method.[19] The Ag and Au atoms were described by a triple-valence-zeta quality basis set with polarization functions (def2-TZVP),[20] employing 28-electron and 60-electron relativistic effective core potentials for Ag and Au, respectively.[21] A split-valence basis set with polarization functions on non-hydrogen atoms was used for all the other atoms (def2-SV(P)).[22] The multipole-accelerated resolution-of-the-identity technique was used to accelerate the calculations.[23] The lowest triplet states of the complexes were studied using spin-unrestricted formalism. The reported computational results were obtained using the observed D_2 point group symmetry to facilitate comparisons with the experiments. All electronic structure calculations were carried out with the TURBOMOLE program package (version 6.1).[24]

RESULTS AND DISCUSSION

Synthesis and Characterization. The synthetic methodology employed for the synthesis of the novel Au^I-Ag^I aggregates is based on the depolymerization reaction of the equimolar amounts of $(AuC_2Ph)_n$ and $(AgC_2Ph)_n$ with the appropriate amount of cationic complex $[Au_2(PP)_2]^{2+}$ that we have communicated recently.[3] Thus, treatment of a slight excess of the mixture of gold and silver acetylides with $[Au_2(\boldsymbol{P^0P})_2]^{2+}$ dimer leads to clean formation of the stable heterometallic cluster $[Au_8Ag_6(C_2Ph)_{12}(\boldsymbol{P^0P})_2]^{2+}$ (**1**; see Scheme 2), which was isolated after repetitious recrystallization as a crystalline solid of bright orange (**1a**) or yellow (**1b**) color (see Figure 1), depending on the solvents used (see the Experimental Section), indicating the existence of different types of crystal structures for **1**.

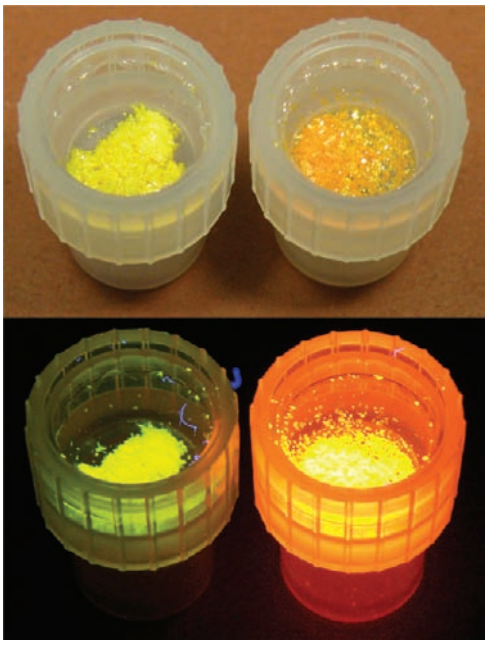

Figure 1. Photographs of the orange (**1a**, right) and yellow (**1b**, left) crystalline forms of **1**, upon exposure to ambient light (top) and UV irradiation (bottom).

Scheme 2. Formation of Cluster 1 (CH_2Cl_2, 12 h, 298 K)

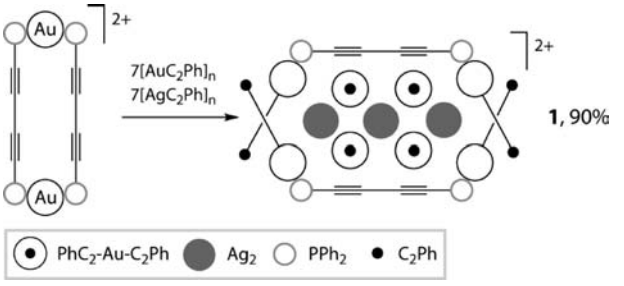

This complex has been studied by ^1H and ^{31}P NMR spectrometry and ESI-MS. Its structure in the solid state (**1a**, orange form) has been determined via XRD analysis (see Figure 2). Unfortunately, the yellow crystalline material was not suitable for X-ray study. The ESI-MS spectrum of **1** (Figure S1 in the Supporting Information, ESI) displays the signal of the doubly charged cation at *m*/*z* 2136.4, the isotopic pattern of which completely fits the stoichiometry of the $[Au_8Ag_6(C_2Ph)_{12}(\boldsymbol{P^0P})_2]^{2+}$ molecular ion.

Complex **1** consists of the heterometallic alkynyl cluster $[Au_4Ag_6(C_2Ph)_8]^{2+}$ placed between two neutral $(PhC_2Au)_2(\mu\text{-}PPh_2C_2C_2PPh_2)$ molecules, which are held together by Au−Au, π−C≡C−Ag and Au−Ag bonds. This general structural arrangement of **1** is similar to that found for **I** (see Scheme 1).[3] The Au−Au bonds between the central framework and external alkynyl-diphosphine fragments (3.0179(3) and 3.0316(3) Å) are typical for aurophilic interactions[4,6,25] and considerably shorter than those found in **I** (3.1247(4) and 3.1973(4) Å).[3] These shorter and evidently more effective

dx.doi.org/10.1021/ic102204h |*Inorg. Chem.* 2011, 50, 2395–2403

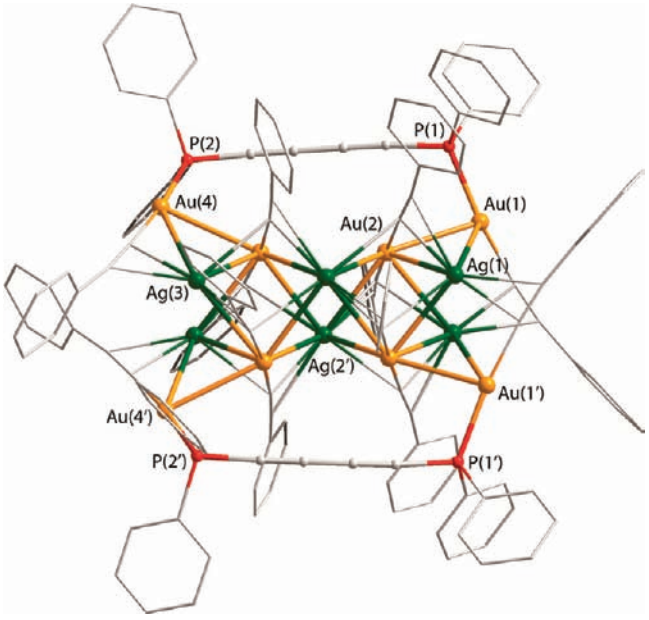

Figure 2. Molecular view of the dication **1a**. Hydrogen atoms omitted for clarity. Selected interatomic distances (Å): Au(1)−P(1), 2.2682(14); Au(1)−Au(2), 3.0179(3); Au(1)−Ag(1), 3.2090(5); Au(2)−Ag(2), 2.9818(5); Au(2)−Ag(1), 3.0279(5); Au(3)−Ag(3), 3.0146(5); Au(3)−Ag(2), 3.0279(5); Au(3)−Au(4), 3.0316(3); Au(4)−P(2), 2.2713(16).

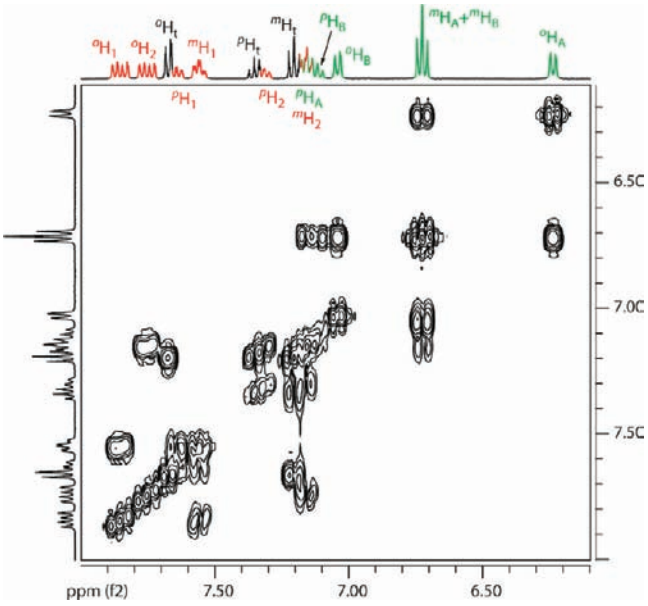

Figure 3. $^{1}H-^{1}H$ COSY spectrum of **1**, CD_2Cl_2, 298 K. Signals of 1D projection marked in red correspond to the phenyl protons of the diphosphines, signals marked in green correspond to the dialkynyl $[Au(C_2Ph)_2]^-$ rods, signals marked in black correspond to the P−Au−C_2Ph terminal fragments.

contacts between the fragments probably determine higher solution stability of **1**, in comparison to **I**; the latter shows signs of degradation within several hours.

The molecular forms of **1a** and **1b** existing in solution were found to be identical. The solution NMR data corresponding to both crystalline forms are consistent with the idealized D_2 symmetry group found in the solid state for **1a**. The ^{31}P NMR spectrum displays a singlet resonance at 16.2 ppm that points to four equivalent P atoms of the diphosphine ligands. The 1D and 2D COSY (Figure 3) proton spectra show well-resolved "ortho−meta−para" groups of the signals corresponding to two sets of inequivalent phenyl rings of the ***P*^0*P*** diphosphine ligand, which are discriminated because of their different orientation, relative to the central core of the complex (see Figure S2 in the Supporting Information). The phenyl resonances of the diphosphine are located in the low field part of the spectrum and display typical $^{31}P-^{1}H$(ortho) coupling constants (ca. 15 Hz) similar to the Au−Ag "rods-in belt" relatives.[6,7] The signals of the phenyl protons of alkynyl ligands are also segregated into a low-field-shifted group of neutral "P−Au−C_2Ph" terminal fragments and two groups of high-field-shifted $[Au(C_2Ph)_2]^-$ rods (see Figure S2 in the Supporting Information).

The use of the linearly extended ligands PPh_2-C_2-$(C_6H_4)_n$-C_2-PPh_2 (n = 1 (***P*^1*P***), 2 (***P*^2*P***), 3 (***P*^3*P***)), employing synthetic protocol similar to the preparation of **1** (Scheme 3), gave the Au^I-Ag^I assemblies of higher nuclearity, $[Au_{10}Ag_8(C_2Ph)_{16}(\boldsymbol{P^1P})_2]^{2+}$ (**2**), $[Au_{12}Ag_{10}(C_2Ph)_{20}(\boldsymbol{P^2P})_2]^{2+}$ (**3**), $[Au_{14}Ag_{12}(C_2Ph)_{24}(\boldsymbol{P^3P})_2]^{2+}$ (**4**), which were isolated as crystalline yellow solids in moderate to excellent yields. Complex **2**, and especially complex **4**, appeared to be unstable in solution at room temperature.

The compositions and structures of the clusters **2**−**4** were elucidated on the basis of ESI-MS and ^{1}H and ^{31}P NMR measurements. The ESI-MS spectra (see Figures S3−S5 in the Supporting Information) display the patterns of the doubly charged molecular ions at m/z 2719.9 (**2**), 3303.0 (**3**), 3885.9 (**4**), which fit the stoichiometry previously given completely. The solid-state structure of **3** has been determined by XRD study. However, the weak diffraction and low quality of the crystals of **3** did not allow for high-quality refinement, but the crystallographic data available, together with the spectral measurements, testify in favor of the structural topology depicted in Scheme 3 (see ESI for the structure determination details and molecular view of the dication **3**; Figure S6 in the Supporting Information).

The proposed structural motif of **2**−**4** is similar to that found for **1** and consists of two alkynyl-diphosphine Au^I molecules $(PhC_2Au)_2(\mu$-PPh_2-C_2-$(C_6H_4)_n$-C_2-$PPh_2)$ (n = 1−3), which accommodate the central clusters $[Au_{4+2n}Ag_{6+2n}(C_2Ph)_{8+4n}]^{2+}$ (see also the computational section below). The NMR spectroscopic characteristics of **2**−**4**, as well as their comparison with the data obtained for **1** and earlier for **I**,[3] strongly support the structural arrangement of the molecules corresponding to the D_2 symmetry group. The singlet resonances in the ^{31}P NMR spectra are indicative of the equivalent P atoms in accordance with the structural pattern suggested in Scheme 3. The position of the phenyl rings of the "belt" diphosphine ligands and those of the P−Au−C_2Ph fragments in the "rods-in-belt" structures of **1**−**4** are not subjected to substantial changes upon growth of the diphosphine spacer length. Because of this, the corresponding NMR signals of these fragments disposed in the low-field part of the proton spectra are almost identical; see Experimental Section, Figure 2, and Figures S7−S9 in the Supporting Information. In turn, the increase in the number of $-C_6H_4-$ moieties within the diphosphine spacers gives additional signals of these fragments in the low-field part of the proton spectra of **2**−**4**. The growth in the diphosphine length gives room for two more $\{Au(C_2Ph)_2\}$ rods per additional phenylene spacer, which results in the appearance of

dx.doi.org/10.1021/ic102204h |*Inorg. Chem.* 2011, 50, 2395–2403

Scheme 3. Formation of Clusters 2−4, x = 8 (P^1P), 10 (P^2P), 12 (P^3P) (CH_2Cl_2, 298 K)

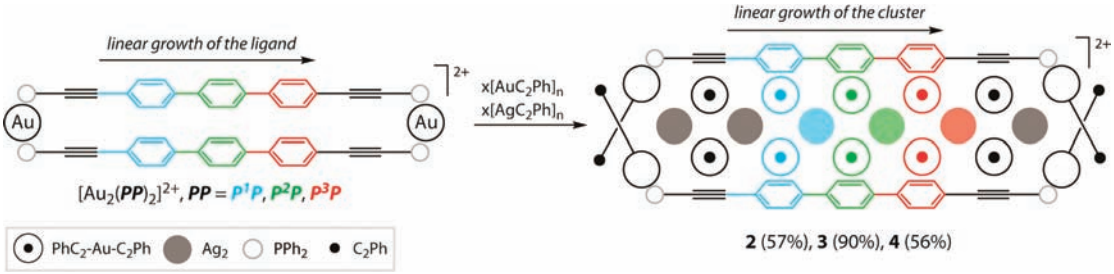

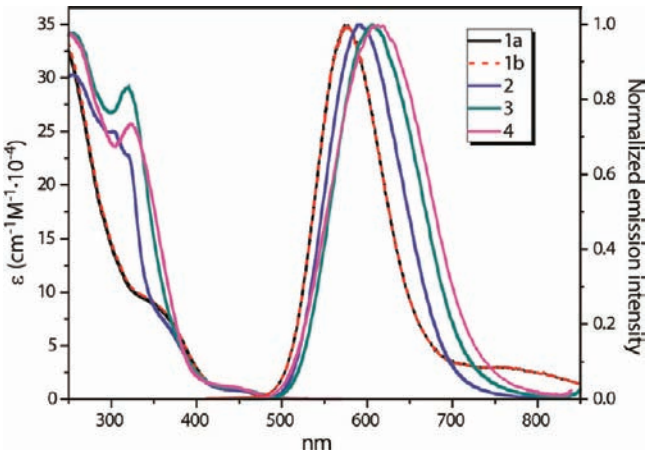

Figure 4. UV/vis absorption and normalized emission spectra of **1**−**4** in aerated CH_2Cl_2 at room temperature, λ_{excit} = 450 nm. Note that absorption and emission taken from batches **1a** and **1b** separately are exactly overlapped.

an additional group of "ortho−meta−para" protons (20H) in the high-field part of the proton spectrum, which can be easily assigned in the corresponding 2D COSY spectrum (see Figures S7−S9 in the Supporting Information). The number of the signals in the proton spectra, as well as their multiplicity and relative intensity, completely fit the structural hypothesis shown in Scheme 3, which supports the validity of the synthetic strategy developed in the present study.

Photophysical Characteristics. Figure 4 shows the UV/vis absorption and emission spectra of complexes **1**−**4** in CH_2Cl_2 at room temperature. Complexes **2**, **3**, and **4** exhibit highly intense, single emission maximized at 592, 606, and 613 nm, respectively, the quantum yield of **2** and **3** being nearly quantitative. As for complex **1**, despite different emission color in solid (vide infra), luminescence for **1a** and **1b** in CH_2Cl_2 is identical, which consists of weak, dual luminescene maximized at 575 (the P_1 band) and 770 nm (the P_2 band). These two bands also undergo the same relaxation dynamics. The analysis of the photophysics of this compound is given in the following sections. All pertinent spectroscopy and dynamics data for **1**−**4** are listed in Table 2. The order of radiative decay rate constant is deduced to be 10^4−10^5 s^{-1}, which suggests the triplet origin of the emissive excited states, i.e., phosphorescence, for all complexes **1**−**4**. Perhaps the most striking feature of the luminescence of the heterometallic clusters is the extremely high emission quantum yield.[26] Moreover, the phosphorescence intensity is almost free from O_2 quenching.[3,4,27] The high quantum yield and negligible O_2 quenching rate manifest the uniqueness of the titled supramolecules framework, in which the emission chromophores (i.e., the central heterometallic alkynyl clusters) are very well-protected by the bulky ancillary and bridging ligands (see Figure 2).

To gain more insight into the spectroscopic features previously discussed, prior to the assignment of the absorption and emission origin, we felt it necessary to execute computational studies to explore the structure−electronic transition relationship. Thus, density functional calculations were performed to shed light on the photophysical behavior of Au(I)−Ag(I) complexes **1**−**4**. The geometries of the complexes were first optimized at the BP86-DFT level of theory. Comparison of the X-ray crystal structure of **1** with the theoretically optimized one showed the Au−Au contacts between the external and central parts to be elongated from 3.02 Å to 3.02−3.20 Å. The difference is most likely due to the fact that the BP86 density functional method is not completely capable of describing closed-shell metal−metal interactions. Furthermore, the lack of the crystal packing effects in the theoretical calculations is expected to result in the deviations observed. However, the general structural motif of clusters **1**−**4** was reproduced well by the theoretical methods, and calibration calculations performed at the experimental geometry showed that the electronic properties of the complexes were not misrepresented because of the structural differences (vide infra).

The frontier molecular orbitals of the S_0 and T_1 electronic states of the Au−Ag complex **1** are illustrated in Figure 5, and the corresponding data for the larger complexes (**2**−**4**) are shown in Figure S10 in the Supporting Information.

For complex **1**, the frontier orbital characteristics calculated at the theoretically optimized geometry were found to be very similar to those calculated for the experimental structural data (see Figure S11 in the Supporting Information). Only one HOMO of the S_0 state is illustrated here, but several lower energy HOMOs were examined to confirm the nature of HOMO. For all complexes, HOMO and LUMO of the S_0 ground state are delocalized over the central fragment. The relaxed geometry of the lowest-energy triplet state T_1 is very similar to the ground state structure for all complexes **1**−**4**. The highest singly occupied molecular orbital (HSOMO), occupied by the excited electron, is closely related to LUMO of the S_0 state, and the lowest singly occupied molecular orbital (LSOMO) is closely related to HOMO of the S_0 state. The fact that both the T_1 LSOMO and HSOMO are composed of alkynyl and metal orbitals of the central fragment suggests that spin−orbit coupling due to the metal orbitals enables efficient radiative decay of the excited triplet state.

dx.doi.org/10.1021/ic102204h |*Inorg. Chem.* 2011, 50, 2395–2403

Table 2. Photophysical Properties of the Au−Ag Complexes in CH_2Cl_2

	λ_{ab} (nm) (10^{-4} ε (cm^{-1} M^{-1}))	λ_{em} (nm)	Φ^a	Φ^b	Φ^c	τ_{obs} (μs)^a	τ_{obs} (μs)^b	τ_{obs} (μs)^c	k_r (s^{-1})^d
1a	351sh (8.8), 447 (0.82)	(575, 770),[a,b] (610)[c]	0.003	0.004	0.28	0.047	0.048	2.64	7.73×10^4
1b	351sh (9.0), 447 (0.83)	(575, 770),[a,b] (570)[c]	0.004	0.004	0.08	0.049	0.049	0.52	8.11×10^4
2	319 (22.8), 329sh (17.9), 360sh (7.5), 449 (0.8)	592 (620)[c]	0.95	1	0.18	5.12	5.3	0.49	1.89×10^5
3	319 (29.0), 450 (1.0)	606 (582)[c]	1	1	0.44	5.41	5.42	1.77	1.85×10^5
4	323 (25.7), 450 (1.1)	613 (550)[c]	0.19	0.19	0.05	2.4	2.4	0.83	7.85×10^4

[a] Measured in aerated CH_2Cl_2. [b] Measured in degassed CH_2Cl_2. [c] Measured in powder. [d] k_r is deduced from data obtained in the degassed solution. 4-Dicyanomethylene-2-methyl-6-*p*-dimethylaminostyryl-4H-pyran (DCM) in methanol was used as a standard for the quantum yield (Φ) measurements. The excitation wavelength is 450 nm for all measurements.

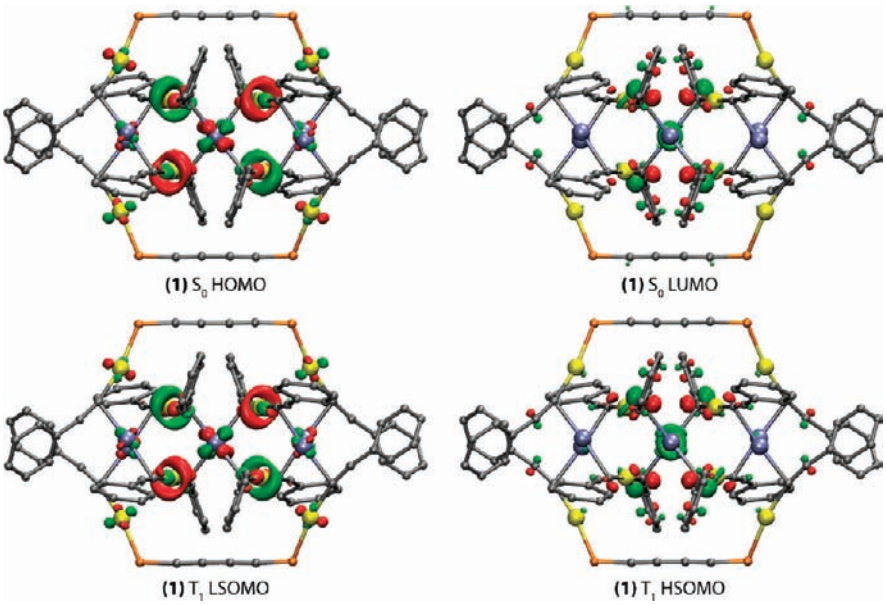

Figure 5. Frontier molecular orbital isodensity plots for complex **1** (isodensity value = 0.04 au). Hydrogen atoms and diphosphine-based phenyl rings have been omitted for clarity.

Standing on the above theoretical basis, the higher-energy absorptions below 300 nm for all of the titled compounds are ascribed to the intraligand $\pi \rightarrow \pi^*$ (C≡C−Ar) transitions inside the alkynyl groups. This assignment is consistent with the previous reports on the relevant alkynyl analogues, for which the dominant absorption band in the spectral region of 230−300 nm is ascribed to the characteristic band of the alkynyl−phosphine fragments. The 300−400 nm absorption bands for these complexes are mainly due to Ag-π-alkynyl fragment metal- and cluster-centered transitions.[2,7] The lowest energy transition extended to ~500 nm, according to the frontier orbital analyses, corresponds to the charge delocalization around metal-alkyne moieties rather than to a pure metal-to-ligand charge transfer (MLCT), because of the mixed feature for both HOMO and LUMO. In solution, all the emission band wavelengths are progressively red-shifted with the increase in the size of the dialkynyl cluster nuclei from 575 nm (the P_1 band) for **1** to 592, 606, and 613 nm for **2**, **3**, and **4**, respectively. However, for the titled heterometallic clusters possessing a massive, flexible framework, the corresponding structure must be subjective to environmental perturbation, resulting in changes of luminescence properties. Particularly, this effect may become dramatic with transfer of the molecules from solution to the rigid solid media, such as in crystal, in which the packing forces should result in freezing of large-amplitude intramolecular motion.

This hypothesis is supported by comparison of the data shown in Figures 4 and 6. In sharp contrast to the bathochromic shift of emission maximum in CH_2Cl_2 solution, **4** > **3** > **2**, the hypsochromic shift of the emission in the order of **4** > **3** > **2** is observed for the crystalline samples, indicating significant structural alternation from solution to solid phase.

Particular attention was paid to the dual emission of the complex **1** in solution. Note that this observation is independent of whether the solution is prepared from solid crystal **1a** or **1b.** Both emission bands are authentic because they possess identical excitation spectra (see Figure S12 in the Supporting Information), which are also overlapping with the absorption spectrum. Accordingly, both 575 and 770 nm emissions originate from the same ground state. Moreover, in solution, both P_1 and P_2 bands have exactly identical relaxation dynamics to give a decay time of ~47 ns at 298 K (Table 3). The assignment of P_1 and P_2 bands to fluorescence and phosphorescence, respectively, has been discarded, because of the much longer radiative decay time (~15 μs, vide supra) deduced. To gain further insight into the dual emission, we also carried out the VT measurements in the temperature range from 298 K to 200 K. The results shown in Table 3 and Figure 7 clearly indicate that P_1 and P_2 bands, within

dx.doi.org/10.1021/ic102204h |*Inorg. Chem.* 2011, 50, 2395–2403

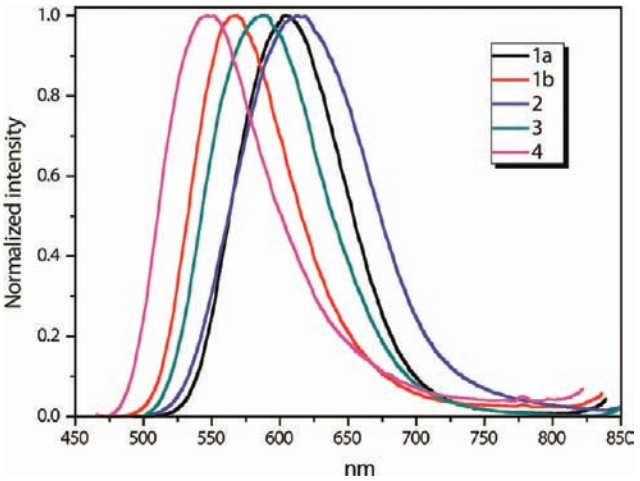

Figure 6. Emission spectra of complexes **1**−**4** in solid state, λ_{ex} = 450 nm.

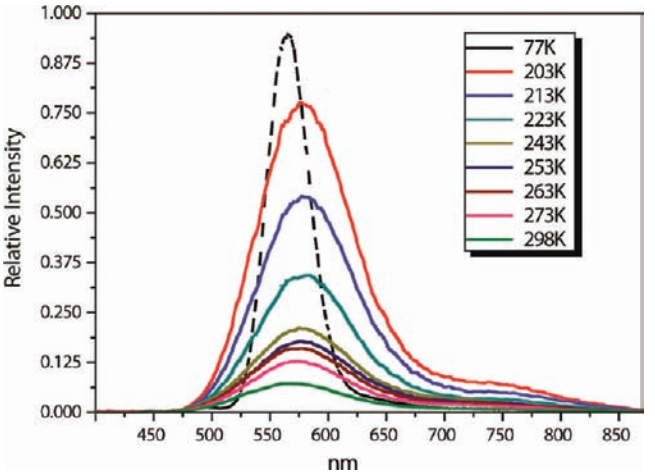

Figure 7. Emission spectra of complex **1a** in degassed CH_2Cl_2 at 298−203 K and 77 K.

Table 3. Photophysical Properties of Complex 1a at Various Temperatures (203−298 K and 77 K) in Degassed CH_2Cl_2

temperature (K)	$\tau(P_1)$ (ns)[a] (575 nm)	$\tau(P_2)$ (ns)[b] (770 nm)	P_1/P_2[c]
77	4150		
203	102.3	101.5	10.5
213	96.6	97.2	10.9
223	92.3	93.1	10.0
233	85.5	83.2	8.15
243	78.3	80.3	7.86
253	75.3	75.8	7.09
263	67.3	68.7	7.23
273	60.2	60.7	7.61
298	47.7	46.3	8.17

[a] Emission monitored at 560 nm. [b] Emission monitored at 760 nm. [c] The ratio of emission intensity for the P_1 band versus the P_2 band.

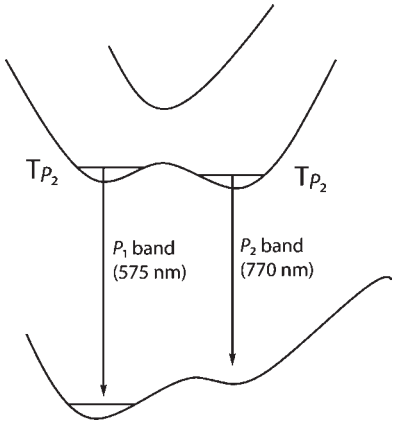

Figure 8. Proposed structural fluctuation between two isomers to account for the observed dual phosphorescence in complex **1**.

experimental error, reveal the same relaxation dynamics as well as an almost-similar intensity ratio for the P_1 versus P_2 band throughout the range of temperatures studied, implying the proximity in energy between two emitting species with a rather small barrier.

Further lowing temperature was not performed due to the system limitation. Nevertheless, upon plunging the sample tube into liquid N_2, only one emission band maximized at ~560 nm is observed at 77 K (Figure 7). Also, the narrower full width at half-maximum (fwhm) is noticed at 77 K, implying large reduction broadening due to the system inhomogeneity.

Summarizing the above experimental results, we herein tentatively propose a rational mechanism based on the existence of two structural conformers, T_{P_1} and T_{P_2} (Figure 8), in the triplet manifold, which respectively render P_1 and P_2 emission. This proposal has its stance in that different crystal packing, as shown in Figure S13 in the Supporting Information, exhibits distinctly different emission, namely single orange−red emission (610 nm) for **1a** and yellow emission (570 nm) for **1b**. Accordingly, it is reasonable to expect that the fluctuation of this heterometallic structure in solution, forming two conformers virtually, may be subject to different intramolecular ligand-to-ligand, metal-to-metal, or even ligand-to-metal interactions. Unfortunately, current experimental and theoretical approaches are unable to provide structural resolution. Although pending resolution, the structural alternation, in part, may associate with the torsional motion along the electronically excited alkynyl-diphosphine moiety, which is thermally unfavorable in the ground state (Figure 8). Since the structural fluctuation does not involve bond breaking/formation, the interconversion between these two conformers must be fast in the fluid phase, as evidenced by the identical relaxation dynamics between the P_1 and P_2 bands. Such structural fluctuation may incorporate large amplitude motions along the reaction coordinate and, hence, is hampered in solid-state media, rationalizing a unique emitting band observed in crystalline samples and the 77 K solid matrix.

As for one of the future perspective, because of the intense (~100% yield) and O_2-quenching-free phosphorescence, complex **3** was also examined for the two-photon absorption (TPA) property. The aim is to explore its application toward nonlinear and time-resolved phosphorescence imaging. Figure S14 in the Supporting Information shows a typical Z-scan and a fitting curve for compound **3** in CH_2Cl_2. As a result, the TPA cross section is calculated to be $\sigma \approx 45$ GM (800 nm) for **3**. The magnitude of this value is similar to that observed for commercially available

TPA dyes such as coumarin 151 ($\sigma \approx 45$ GM at 800 nm),[28] making **3** promising as a two-photon absorption phosphorescence dye.

CONCLUSION

In conclusion, a new family of heterometallic aggregates **1**−**4** has been designed and synthesized via self-organization of the mixture of $(AuC_2Ph)_n$ and $(AgC_2Ph)_n$ polymers upon treatment with cationic complexes $[Au_2(PPh_2\text{-}C_2\text{-}(C_6H_4)_n\text{-}C_2\text{-}PPh_2)_2]^{2+}$ (n = 0, 1, 2, 3). Several intriguing and significant remarks can be noted. In the solid, complex **1** exists as two crystalline forms (**1a** and **1b**) with different colors and different associated emissions. In solution, this compound exhibits dual phosphorescence in the yellow and near-infrared region. The results lead to a conclusion that **1**, upon excitation, undergoes fast structural fluctuation, forming virtually two conformers in equilibrium, which accounts for the dual emission. Complexes **2** and **3** demonstrate intense phosphorescence with unity quantum efficiency. An equally important point is that the phosphorescence, although having a lifetime as long as 5−6 μs, does not display O_2 quenching. The result evidently manifests the uniqueness of their framework, in which the emission chromophores—the central heterometallic alkynyl clusters—are protected by the bulky ancillary and bridging ligands from the dipole interaction with molecular oxygen.

ASSOCIATED CONTENT

Supporting Information. X-ray crystallographic data in CIF for **1**, $^1H-^1H$ COSY spectra of **2**−**4**, ESI-MS spectra of **1**−**4**, additional theoretical data, and optimized Cartesian coordinates of the studied systems in atomic units. This material is available free of charge via the Internet at http://pubs.acs.org.

AUTHOR INFORMATION

Corresponding Author

*E-mails: igor.koshevoy@uef.fi (I.O.K.), chop@ntu.edu.tw (P.-T.C.), and tapani.pakkanen@uef.fi (T.A.P.).

ACKNOWLEDGMENT

Financial support from the Academy of Finland (I.O.K.), European Union/European Regional Development Fund (Grant No. 70026/08 (A.J.K. and I.O.K.)), and Russian Foundation for Basic Research (Grant No. 09-03-12309 ofi-m) and Federal Agency on Science and Innovations (FC 02.518.11.7140) is gratefully acknowledged.

REFERENCES

(1) (a) Gimeno, M. C.; Laguna, A. *Chem. Soc. Rev.* **2008**, *37*, 1952–1966. (b) Fernandez, E. J.; Laguna, A.; Lopez-de-Luzuriaga, J. M. *Dalton Trans.* **2007**, 1969–1981.

(2) Koshevoy, I. O.; Koskinen, L.; Haukka, M.; Tunik, S. P.; Serdobintsev, P. Y.; Melnikov, A. S.; Pakkanen, T. A. *Angew. Chem., Int. Ed.* **2008**, *47*, 3942–3945.

(3) Koshevoy, I. O.; Lin, Y.-C.; Karttunen, A. J.; Haukka, M.; Chou, P.-T.; Tunik, S. P.; Pakkanen, T. A. *Chem. Commun.* **2009**, 2860–2862.

(4) Koshevoy, I. O.; Lin, Y.-C.; Chen, Y.-C.; Karttunen, A. J.; Haukka, M.; Chou, P.-T.; Tunik, S. P.; Pakkanen, T. A. *Chem. Commun.* **2010**, *46*, 1440–1442.

(5) (a) Schuster, O.; Monkowius, U.; Schmidbaur, H.; Ray, R. S.; Kruger, S.; Rosch, N. *Organometallics* **2006**, *25*, 1004–1011. (b) Koshevoy, I. O.; Karttunen, A. J.; Tunik, S. P.; Haukka, M.; Selivanov, S. I.; Melnikov, A. S.; Serdobintsev, P. Y.; Khodorkovskiy, M. A.; Pakkanen, T. A. *Inorg. Chem.* **2008**, *47*, 9478–9488.

(6) Koshevoy, I. O.; Karttunen, A. J.; Tunik, S. P.; Haukka, M.; Selivanov, S. I.; Melnikov, A. S.; Serdobintsev, P. Y.; Pakkanen, T. A. *Organometallics* **2009**, *28*, 1369–1376.

(7) Koshevoy, I. O.; Ostrova, P. V.; Karttunen, A. J.; Melnikov, A. S.; Khodorkovskiy, M. A.; Haukka, M.; Jänis, J.; Tunik, S. P.; Pakkanen, T. A. *Dalton Trans.* **2010**, *39*, 9022–9031.

(8) (a) Abu-Salah, O. M.; Knobler, C. B. *J. Organomet. Chem.* **1986**, *302*, C10–C12. (b) Wei, Q.-H.; Zhang, L.-Y.; Yin, G.-Q.; Shi, L.-X.; Chen, Z.-N. *Organometallics* **2005**, *24*, 3818–3820. (c) Wei, Q.-H.; Zhang, L.-Y.; Yin, G.-Q.; Shi, L.-X.; Chen, Z.-N. *J. Am. Chem. Soc.* **2004**, *126*, 9940–9941.(d) Silvestru, C. In *Modern Supramolecular Gold Chemistry*; Laguna, A., Ed.; Wiley−VCH: Weinheim, Germany, 2008; pp 181−295.

(9) Coates, G. E.; Parkin, C. *J. Chem. Soc.* **1962**, 3220–3226.

(10) Teo, B. K.; Xu, Y. H.; Zhong, B. Y.; He, Y. K.; Chen, H. Y.; Qian, W.; Deng, Y. J.; Zou, Y. H. *Inorg. Chem.* **2001**, *40*, 6794–6801.

(11) (a) Xu, D.; Hong, B. *Angew. Chem., Int. Ed.* **2000**, *39*, 1826–1829. (b) Corriu, R. J. P.; Guérin, C.; Henner, B. J. L.; Jolivet, A. *J. Organomet. Chem.* **1997**, *530*, 39–48.

(12) Merkushev, E. B.; Yudina, N. D. *Zh. Org. Khim.* **1981**, *17*, 2598–2601.

(13) Sheik-Bahae, M.; Said, A. A.; Wei, T.-H.; Hagan, D. J.; Van Stryland, E. W. *IEEE J. Quantum Electron.* **1990**, *26*, 760–769.

(14) Fisher, W. G.; Wachter, E. A.; Lytle, F. E.; Armas, M.; Seaton, C. *Appl. Spectrosc.* **1998**, *52*, 536–545.

(15) *APEX2—Software Suite for Crystallographic Programs*; Bruker AXS, Inc.: Madison, WI, 2009.

(16) Sheldrick, G. M. *Acta Crystallogr., Sect. A: Found. Crystallogr.* **2008**, *A64*, 112–122.

(17) Farrugia, L. J. *J. Appl. Crystallogr.* **1999**, *32*, 837–838.

(18) Sheldrick, G. M. *SADABS-2008/1—Bruker AXS area detector scaling and absorption correction*; Bruker AXS, Inc.: Madison, WI, 2008.

(19) (a) Becke, A. D. *Phys. Rev. A* **1988**, 3098–3100. (b) Vosko, S. H.; Wilk, L.; Nusair, M. *Can. J. Phys.* **1980**, *58*, 1200–1211. (c) Perdew, J. P. *Phys. Rev. B* **1986**, *33*, 8822–8824.

(20) Weigend, F.; Ahlrichs, R. *Phys. Chem. Chem. Phys.* **2005**, *7*, 3297–3305.

(21) Andrae, D.; Häussermann, U.; Dolg, M.; Stoll, H.; Preuss, H. *Theor. Chem. Acc.* **1990**, *77*, 123–141.

(22) Schäfer, A.; Horn, H.; Ahlrichs, R. *J. Chem. Phys.* **1992**, *97*, 2571–2577.

(23) (a) Eichkorn, K.; Treutler, O.; Öhm, H.; Häser, M.; Ahlrichs, R. *Chem. Phys. Lett.* **1995**, *240*, 283–290. (b) Sierka, M.; Hogekamp, A.; Ahlrichs, R. *J. Chem. Phys.* **2003**, *118*, 9136–9148. (c) Eichkorn, K.; Weigend, F.; Treutler, O.; Ahlrichs, R. *Theor. Chem. Acc.* **1997**, *97*, 119–124. (d) Weigend, F. *Phys. Chem. Chem. Phys.* **2006**, *8*, 1057–1065.

(24) Ahlrichs, R.; Bär, M.; Häser, M.; Horn, H.; Kölmel, C. *Chem. Phys. Lett.* **1989**, *162*, 165–169.

(25) Pyykko, P. *Angew. Chem., Int. Ed.* **2004**, *43*, 4412–4456.

(26) (a) Crespo, O.; Gimeno, M. C.; Laguna, A.; Larraz, C.; Villacampa, M. D. *Chem.—Eur. J.* **2007**, *13*, 235–246. (b) Jia, J.-H.; Wang, Q.-M. *J. Am. Chem. Soc.* **2009**, *131*, 16634–16635. (c) Manbeck, G. F.; Brennessel, W. W.; Stockland, J.; Robert, A.; Eisenberg, R. *J. Am. Chem. Soc.* **2010**, *132*, 12307–12318.

(27) Koshevoy, I. O.; Lin, Y.-C.; Karttunen, A. J.; Chou, P.-T.; Vainiotalo, P.; Tunik, S. P.; Haukka, M.; Pakkanen, T. A. *Inorg. Chem.* **2009**, *48*, 2094–2102.

(28) Fischer, A.; Cremer, C.; Stelzer, E. H. K. *Appl. Opt.* **1995**, *34*, 1989–2003.